Lab on a Chip

An Autonomous Wearable System for Diurnal Sweat Biomarker Data Acquisition

Journal:	*Lab on a Chip*
Manuscript ID	LC-ART-08-2020-000820.R1
Article Type:	Paper
Date Submitted by the Author:	21-Sep-2020

Complete List of Authors:	Hojaiji, Hannaneh; University of California Los Angeles Henry Samueli School of Engineering and Applied Science, Electrical and Computer Engineering Zhao, Yichao; University of California Los Angeles Gong, Max; University of California Los Angeles Henry Samueli School of Engineering and Applied Science, Electrical and Computer Engineering Mallajosyula, Mudith; University of California Los Angeles Henry Samueli School of Engineering and Applied Science, Computer Science and Engineering Tan, Jiawei; University of California Los Angeles, Materials Science and Engineering Lin, Haisong; University of California Los Angeles Henry Samueli School of Engineering and Applied Science, Electrical and Computer Engineering Hojaiji, Amir; Interconnected and Integrated Bioelectronics Lab, University of California, Los Angeles Lin, Shuyu; University of California Los Angeles, Electrical and Computer Engineering Milla, Carlos; Stanford University School of Medicine, The Stanford Cystic Fibrosis Center, Center for Excellence in Pulmonary Biology Madni, Asad; University of California Los Angeles Henry Samueli School of Engineering and Applied Science, Electrical and Computer Engineering Emaminejad, Sam; University of California Los Angeles Henry Samueli School of Engineering and Applied Science, Electrical and Computer Engineering

An Autonomous Wearable System for Diurnal Sweat Biomarker Data Acquisition

Hannaneh Hojaiji [1,2†], Yichao Zhao [1,3†], Max C. Gong [1,2], Mudith Mallajosyula [1, 4], Jiawei Tan[1,3], Haisong Lin [1,2], Amir M. Hojaiji [1], Shuyu Lin [1,2], Carlos Milla [5], Asad M. Madni [2], and Sam Emaminejad [1, 2, 6]*

[1] Interconnected and Integrated Bioelectronics Lab (I^2BL), Henry Samueli School of Engineering and Applied Science, University of California, Los Angeles, CA, USA

[2] Department of Electrical and Computer Engineering, University of California, Los Angeles, CA, USA

[3] Department of Materials Science and Engineering, University of California, Los Angeles, CA, USA

[4] Department of Computer Science and Engineering, University of California, Los Angeles, CA, USA

[5] The Stanford Cystic Fibrosis Center, Center for Excellence in Pulmonary Biology, Stanford School of Medicine, Stanford, CA, USA

[6] Department of Bioengineering, University of California, Los Angeles, CA, USA

† *These authors contributed equally to this work.*

* *Correspondence and requests for materials should be addressed to S.E. (emaminejad@ucla.edu)*

Abstract

To track dynamically varying and physiologically relevant biomarker profiles in sweat, autonomous wearable platforms are required to periodically sample and analyze sweat with minimal or no user intervention. Previously reported sweat sensors are functionally limited to capturing biomarker information at one time-point/period, thereby necessitating repeated user intervention to increase the temporal granularity of biomarker data. Accordingly, we present a compact multi-compartment wearable system, where each compartment can be activated to autonomously induce/modulate sweat secretion (*via* iontophoretic actuation) and analyze sweat at set time points. This system was developed following a hybrid-flex design and a vertical integration scheme—integrating the required functional modules: miniaturized iontophoresis interfaces, adhesive thin film microfluidic-sensing module, and control/readout electronics. The system was deployed in a human subject study to track the diurnal variation of sweat glucose levels in relation to the daily food intake. The demonstrated autonomous operation for diurnal sweat biomarker data acquisition illustrates the system's suitability for large-scale and longitudinal personal health monitoring applications.

Introduction

Wearable biomarker sensing platforms are poised to catalyze the transition from point-of-lab and point-of-care to point-of-person health and wellness monitoring as they provide frequent, real-time, and contextually relevant measures of informative biomarker molecules. Among the potential wearable solutions, sweat-based sensing modality particularly allows for accessing biomarker molecules non-invasively. Accordingly, various sweat bioanalytical platforms were developed (typically implemented as a disposable biochemical sensor unit interfacing a control/readout circuit module) and utilized to target biomarker molecules such as metabolites, electrolytes, and nutrients [1-5]. However, the presented platforms are functionally limited to one time-point/period biomarker data recording. To acquire biomarker information at multiple points during the day, frequent thermal/exercise-based or iontophoresis-based (manually set up) sessions are required to access sweat, and pristine microfluidic/sensor unit replacements are necessary to avoid sample/sensor contamination. Therefore, the underlying limitations of such wearable sweat platforms prohibit their translation into large-scale and longitudinal personal health monitoring applications [1-12].

Here, to address such limitations, we devise a multi-compartment wearable system, where each compartment can be programmatically activated to induce/modulate sweat secretion (*via* iontophoretic actuation) and analyze sweat at intermittent time-points. This system was realized within a compact footprint, following an introduced hybrid-flex system design and seamless integration methodology—integrating the required functional modules: 1) an array of iontophoretic actuation interfaces, where each interface can be independently programmed to activate/modulate sweat secretion; 2) a laser-patterned thin tape-based microfluidic module for sweat sampling and routing; 3) electrochemical sensing interfaces, which are functionalized on an

anisotropic conductive adhesive (ACA) substrate to facilitate seamless biomarker signal transduction to the electronics within the microfluidic module; and 4) a kirigami-inspired and multi-layered flexible printed circuit board (FPCB) to execute system-level functionalities, including tunable iontophoresis (to modulate secretory agonist delivery and thus sweat secretion), sensor signal acquisition/processing, and biomarker data display/wireless transmission.

As a self-sufficient solution, the integrated hybrid-flex wearable system realizes core functionalities such as sweat stimulation at the desired time and secretion rate, *in-situ* signal processing, real-time data display, and bidirectional data communication with phone/cloud server. By automating these operations, delivered within the devised multi-compartment configuration, we enabled the tracking of the diurnal profile of glucose, as an illustrative biomarker with clinical significance.

Materials and methods

Characterization of the programmable iontophoresis (delivered by the hybrid-flex system)

The programmable iontophoresis characterization and diurnal human subject studies were performed with our wearable system. The commercial agonist-loaded hydrogel discs (0.5% pilocarpine nitrate, [13], PILOGEL®, Wescor Inc., South Logan, Utah) were reshaped (using custom-designed 3D printed molds) to fit the semi-annular positive iontophoresis electrode array. The programmable iontophoretic stimulation was then performed following the sweat stimulation settings described in the results section.

Sweat secretion rate characterization using standard lab instruments

The capability to program sweat secretion rate was first examined (Fig. 2e, f) using standard lab instruments. Pilocarpine hydrogels (1% pilocarpine nitrate) were fabricated, following the previously introduced method [14]. These hydrogels were molded into donut-shaped gels (area: 3.2 cm^2), and were used to iontophoretically stimulate sweat on the volar surface of the two forearms (alternating between the two arms at each point) for the two subjects using a commercial Q-sweat system (WR Medical Electronics Co. Maplewood, MN). By varying the applied current and duration of iontophoresis, the iontophoretic dosage was tuned for each stimulation datapoint. The commercial sweat-rate sensor (Q-sweat, WR Medical Electronics Co.) was mounted onto the skin, at the center (area: 0.8 cm^2) of the donut-shaped positive electrode, to measure sweat secretion rate for the corresponding iontophoretic dosage. The sweat secretion rate was continuously measured for 10 minutes from the time of the stimulation started and data points represent the plateau of the sweat rate.

Electrochemical sensor design and characterization

To fabricate thin-film electrochemical sensors, first, gold (Au) was deposited and patterned on an ACA substrate (9703, 3M, 50 μm). Then, platinum nanoparticles (PtNP) were electro-deposited onto the ACA/Au [15]. The biosensing interface was constructed by electrochemically depositing poly-*m*-phenylenediamine (PPD) layer onto the PtNP/Au/ACA by applying + 0.85 V (*vs*. Ag/AgCl) for 300 s in a fresh phosphate-buffered saline solution (Gibco® PBS, ThermoFisher, pH 7.2) with 5 mM *m*-phenylenediamine (Sigma-Aldrich). A 1% chitosan solution was thoroughly mixed with a glucose oxidase solution (Sigma-Aldrich, 50 mg/mL in PBS, pH 7.2) at a ratio of 1:1 (volume/volume). The glucose sensing interface was realized by drop-casting 1 μL of the aforementioned mixture onto the PPD/PtNP/Au/ACA electrode (4 mm^2) [16]. To create the lactate sensor, a 4 μL lactate oxidase solution (Toyobo, 50 mg/mL in PBS) was deposited onto PtNP/Au/ACA electrode and dried at room temperature, followed by drop-casting of a 2 μL 1% Chitosan solution and a 2 μL 3% polyvinyl chloride (PVC, Sigma-Aldrich) solution. To characterize the developed electrochemical sensor, constant potential amperometric measurements were conducted at + 0.3 V *vs*. Ag/AgCl. The amperometric response was recorded by a potentiostat (CHI 660E) or the custom-developed PCB. By drop-casting different concentrations of the target analytes onto the sensors' surface, a series of calibration curves were obtained. The sensor selectivity tests were performed in PBS buffer (pH 7.2) by the stepwise addition of different interfering species and glucose into PBS.

Fabrication and assembly of microfluidic-sensing module

The thin film microfluidic-sensing module consists of an ACA-based sensing layer, a microfluidic structure layer (170 μm-thick, 9474LE double-sided tape, 3M), polyethylene

terephthalate (PET, MG Chemicals, ~100 μm), a skin adhesive layer (170 μm-thick, 9474LE double-sided tape, 3M), and a filler layer (Scotch single-sided self-seal laminating sheets, 3M, USA). We use a laser-cutter (VLS2.30, Universal Laser Systems) to form 2D patterns of microfluidic channels/chambers in the microfluidic structure and skin adhesive layers, and biofluid inlets (d = 0.5 mm) in the PET and filler layers. The microfluidic-sensing module was assembled by vertically stacking these layers. On one side, the module adheres to the FPCB through the ACA layer, and on the other side, adheres onto skin through the skin adhesive layer. Additionally, the skin adhesive layer (the flap-like patterns) also supports the hydrogel (within a 3D printed encapsulated mold) array interfacing with the skin.

The hybrid-flexible FPCB module

At its core, the electronic module houses a microcontroller (MCU) unit (STM8L – UFQFN20, STMicroelectronics). The MCU was programmed to facilitate system-level functionalities (*i.e.* controlling the iontophoresis and sensing circuitries), data analysis, signal transduction through Bluetooth, and plotting the signal readouts on an onboard LCD screen (st7735 – TFT-LCD, Sitronix Technology Corporation) in real-time. A programmable current source based on a unity-gain difference amplifier (AD8276 – 8MSOP, Analog Devices) was designed to realize tunable iontophoretic actuation. This current source was integrated with an overcurrent protection circuitry using a current shunt monitor (INA282 – 8SOIC, Texas Instruments) as well as software and hardware current control mechanisms that utilize the MCU's Analog-to-Digital (ADC) and Digital-to-Analog (DAC) modules (controlled programmatically on the MCU and through the custom-developed smartphone application). With on-demand switching capabilities, the onset of iontophoresis activation at each compartment was actively controlled. A potentiostat chip (LMP91000, Texas Instruments) was programmed to

generate and maintain the + 0.3 V potential across the sensing electrodes and continuously measure the amperometric output of the sensor (~ 40 minutes, after sweat stimulation before/after each meal intake). The analog-front-end in this circuit converted the measured current to voltage. To mitigate the interfering high-frequency noise, the output voltage was filtered out through a fifth-order low pass filter (MAX7422 chip – Maxim Integrated, LPF) with a cut off frequency of 1 Hz.

Human subject testing and institutional review board (IRB) approval

The conducted human subject experiments were performed in compliance with the protocols approved by the Institutional Review Board (IRB) at the University of California, Los Angeles (no. 17-000170) and the IRB at Stanford University (no. 31310). Healthy subjects were recruited based on the approved IRB protocols. All subjects gave written informed consent before participation in the study. Prior to the on body experiments, the forearm was cleaned with isopropyl alcohol (Sigma-Aldrich), rinsed with deionized (DI) water, and wiped with Kimwipes (Kimtech Science), followed by mounting the device on the forearm. For *in-situ* sample analysis, amperometry recording began after 5 minutes of iontophoresis, and following a 10-minute wait-time for the initiation of sweat secretion. The corresponding biomarker data was taken after a ~ 30-minute wait-time to ensure sufficient sweat sample accumulation (for reliable analysis).

Results and Discussion

Design and operational principle of the hybrid-flex system

The skin adherable hybrid-flex system (Fig. 1a) is realized following a vertical integration scheme, integrating various functional modules: miniaturized iontophoresis interfaces, adhesive thin film microfluidic-sensing module, and control/readout electronics (Fig. 1b). The system is implemented as a kirigami-inspired multi-compartment configuration, where linear incisions—in hexagonal-shaped FPCB and microfluidic-sensing modules—were utilized to render flap-like compartments, thus providing the mechanical degree of freedom necessary for structural compliance with skin. In this configuration, each compartment can be individually addressed to induce/modulate sweat secretion (*via* iontophoretic actuation) and analyze sweat at set time-points (Fig. 1c).

The iontophoretic sweat induction is achieved with the aid of a digitally programmable current source and a miniaturized iontophoresis electrode/hydrogel array. This implementation allows for the tunable delivery of secretory agonist molecules (embedded in hydrogel) underneath the skin, simply by adjusting the iontophoresis current level/duration, thus enabling the modulation of the sweat secretion profile. In our design, the iontophoresis electrodes are monolithically integrated within the FPCB module: the positive semi-annular electrodes fabricated on the backside of the FPCB flaps, radially arranged around a shared circular negative electrode (on the backside of the center of FPCB). Furthermore as shown in Fig. 1c, the semi-annular design of the positive iontophoresis electrodes facilitates a lateral pathway [5] for the stimulation of neighboring sweat glands (that are vertically below sweat sampling microfluidic interface, but laterally away

from the iontophoresis interface). The collection and analysis of secreted sweat is achieved with the aid of a thin-film microfluidic-sensing module, featuring an array of microfluidic sensing chambers, (Fig. S1) where each sensing chamber is paired with an iontophoresis interface. The sensing interfaces are engineered on an ACA film. In this way, the adhesive and vertical conductivity of the film can be exploited to interconnect the transduced signal to the readout circuitry of the FPCB, *in-situ*, *via* monolithically integrated sensing contact pads. By programming the FPCB, the compartments within our system can be activated at set time points during the day to render biomarker readings autonomously and non-invasively. Therefore, as conceptualized in Fig. 1d, the devised solution presents great potential to facilitate longitudinal monitoring of biomarkers across the general population.

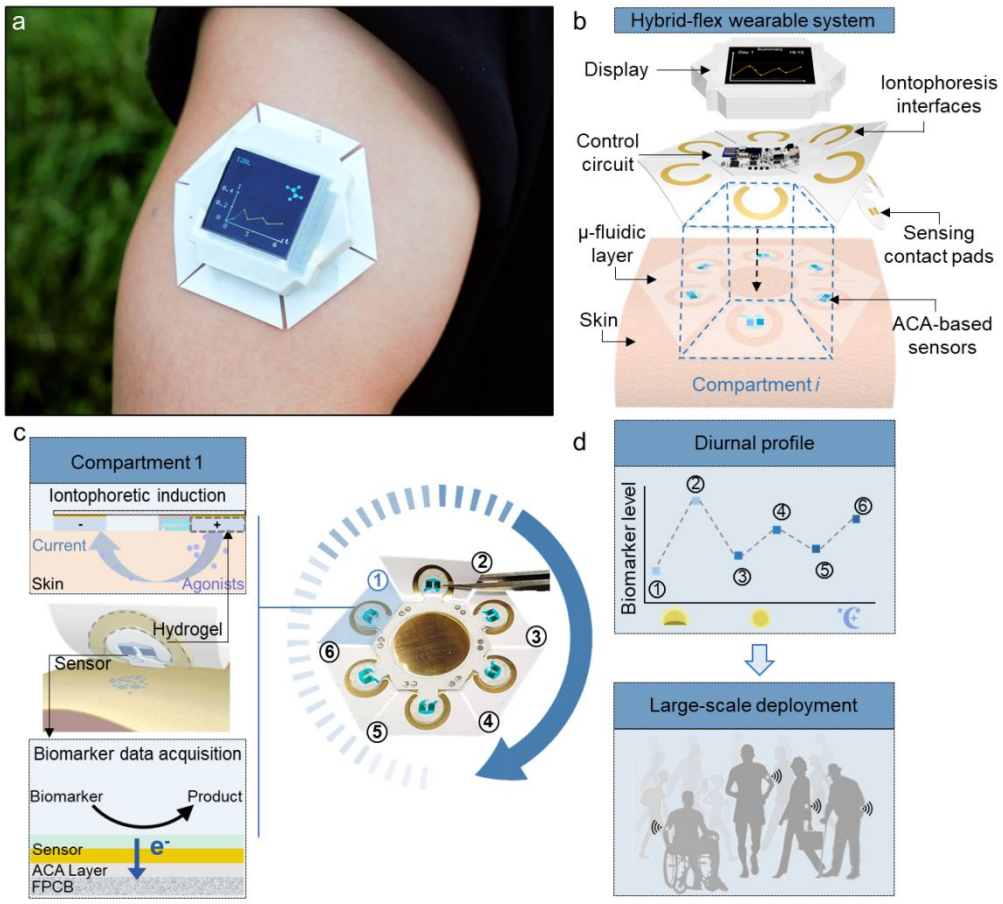

Figure 1. Design and operational principle of the hybrid-flex wearable system: a) Image of the developed hybrid-flex wearable system adhered on a subject's arm; b) Exploded schematic of the multi-compartment system, demonstrating vertical integration of an FPCB with iontophoresis electrode arrays (radially fabricated on the backside of the FPCB) and a microfluidic-sensing module; c) Schematic representation of bioanalytical operations (left: iontophoresis, sensing) delivered by each of the compartments (right: bottom view photograph of the developed hybrid-flex wearable system) that can be programmatically activated at intermittent time points to obtain biomarker data; d) Conceptual illustration of positioning the autonomous system to track the diurnal biomarker profiles for population-level health monitoring.

Miniaturized and programmable iontophoresis interface for sweat secretion modulation

First, the robustness of the iontophoresis current delivery under mechanical deformation was tested under three iontophoresis electrode bending conditions (flat; $\alpha = 60°$, $R = 15$ mm; and $\alpha = 30°$, $R = 10$ mm, Fig. 2a), where the applied iontophoretic current was continuously monitored. The results demonstrate that the effect of bending on iontophoresis current was negligible (Fig. 2b). Then, the consistency of the iontophoretic operations across all six compartments and for different physiologically relevant skin conditions (~300 Ω to ~100 kΩ [17]) was evaluated, *ex situ*, by monitoring the applied current through representative skin impedance loads. As shown in Fig. 2c, the iontophoresis current differences across all six compartments were less than 0.9% (R_{skin} = 47 kΩ). Similarly, the variation in the load impedances had minimal effect on the delivered current level (Fig. 2c inset). To evaluate the stability of on-body iontophoresis stimulation by our wearable system, we performed iontophoresis in the presence of body motions with different intensities. Figure 2d illustrates a stable iontophoresis current profile (negligible current fluctuation, coefficient of variation (CV) < 2%) was delivered under varying body motion frequencies and accelerations (from ~0 to ~20 Hz, and from ~0 to ~20 m/s^2 respectively).

By capitalizing on the capability of our system in tuning the iontophoresis current level and duration of the stimulation, we can control the amount of agonists delivered to the glands, thus allowing us to effectively program the secretion profile and adjust the secretion rate/volume. In our iontophoretic setup, the amount of agonist (P), can be estimated to the first order by the equation below, which illustrates the proportionality of P to the product of the stimulation current I and duration t:

$$P = \frac{I\,t\,M}{F} \qquad (1)$$

Where F is the Faraday constant (96489 C/mol) and M is the molecular weight of the agonist (*i.e.* 271 g/mol), I in mA, and t in seconds [18].

To examine our ability to program the secretion rate, first, we performed sweat stimulation (utilizing standard lab instruments) on two subjects, where in each of the cases we varied I and t (I = 0.5, 1 mA; t = 3, 5 min). As shown in Fig. 2e, f, our sweat secretion characterization results (performed with an evaporimeter) illustrated that higher $I \times t$ conditions (iontophoretic stimulation dosage) led to higher secretion rates for both subjects. We can also exploit our programmable sweat induction capability to ensure harvesting sufficient sweat sample volumes for reliable *in-situ* analysis. To illustrate this point, using our solution, we performed sweat stimulation (two trials) with different iontophoresis current levels and fixed duration (on nearby spots of the volar surface of the subject's arm) and secretion characterization with a spiral-shaped microfluidic sweat collector (Fig. S2a). As shown in Fig. 2g, for both trials, the increased iontophoresis current led to larger secreted sweat sample volumes. Furthermore, we can exploit our programmable sweat induction capability to elicit sweat secretion at desired time-points during the day, which is instrumental in the envisioned diurnal biomarker monitoring application. To illustrate this point, we deployed our multi-compartment system in a human subject study, where we programmed the compartments to be activated at different time points to induce sweat. As illustrated in Fig. 2h, sufficient sweat sample volume (> 2 μL) was consistently induced across the six compartments during a day. We further verified that the accumulation of sweat due to natural perspiration over an extended amount of time (> 7 hours) and upon a moderate elevation in ambient temperature (6 °C) is negligible (Fig. S2b, c). To avoid contamination of sensors due to sweat induction by non-iontophoretic mechanisms (*e.g.*, physical exercise), electronically-programmable microfluidic valves [19, 20] can be incorporated at the entry points of the sensing chambers.

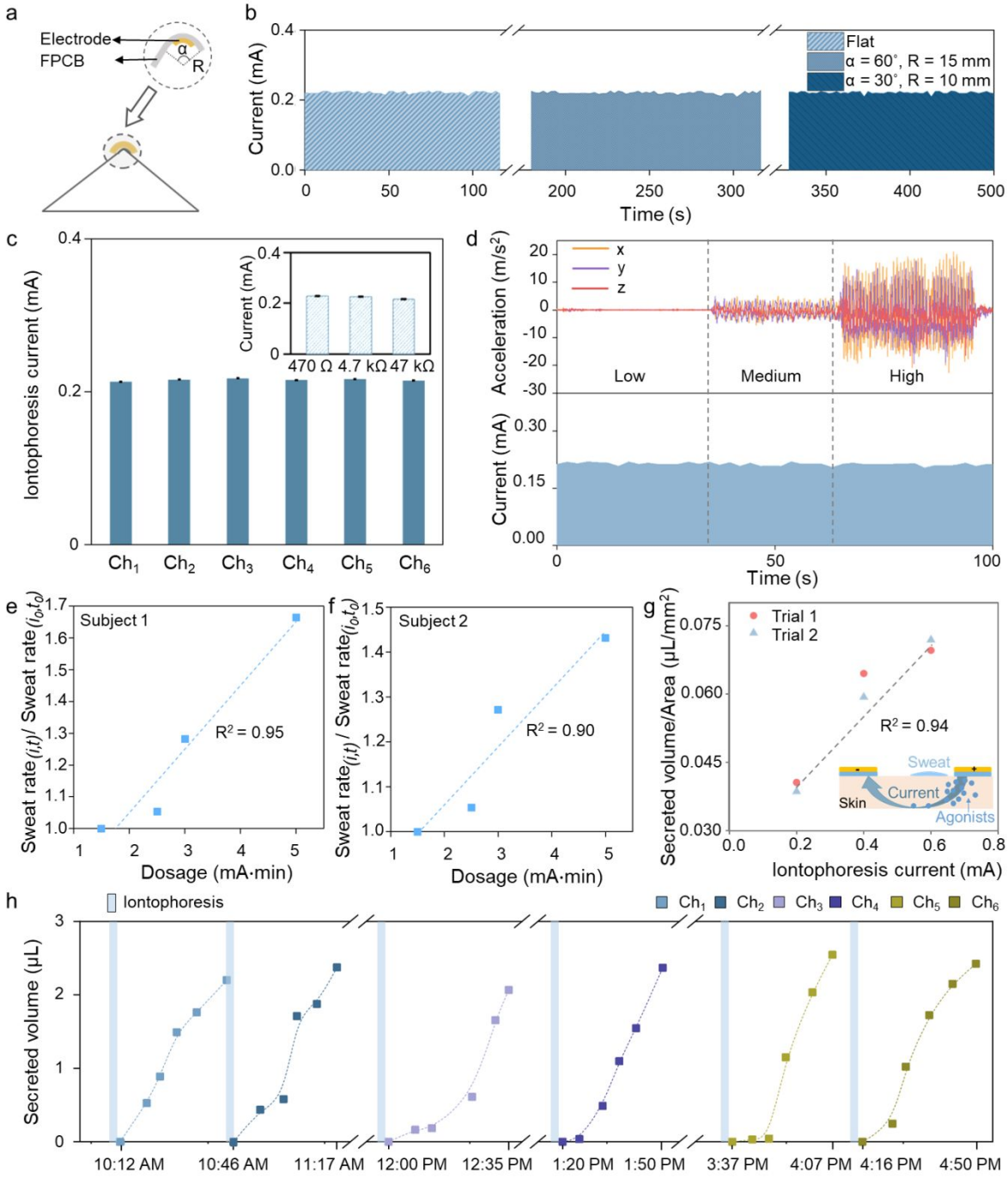

Figure 2. Characterization of the miniaturized and programmable iontophoresis: a) Illustration of the setup for iontophoresis current characterization, performed under three bending conditions (1. no bending, 2. α = 60°, R = 15 mm, and 3. α = 30°, R = 10 mm); b) Real-time iontophoresis current recordings under corresponding bending conditions (programmed current: 0.2 mA, CV for all cases < 1.5%); c) Demonstration of consistent iontophoresis current delivery

across all compartments (load: 47 kΩ, programmed current: 0.2 mA, Δ = 0.9%). Inset shows load-independent iontophoresis current delivery capability of the system. Error bars indicate standard error (n = 6 compartments). Δ is calculated as percent variation of the maximum measured current level from the baseline average value; d) *In-situ* characterization of iontophoresis current stability on body under different exercise intensities (programmed current: 0.2 mA); e, f) Sweat secretion rate *vs.* iontophoretic dosage for subject 1 (e) and 2 (f). The normalized sweat rate is obtained by dividing the measured sweat rate with the iontophoretic dosage ($I_n \times t_n$) by the sweat rate with the dosage ($I_0 \times t_0$) = (0.5 mA × 3 min); g) Tunable sweat secretion rate achieved by programming the iontophoresis current (rendered by our wearable platform, area of stimulation: 0.64 cm^2, corresponding to a current density of ~ 0.3 mA/cm^2 for I_0 = 0.2 mA). Inset shows the iontophoretic sweat agonist delivery process; h) Intermittent sweat induction throughout a day using six sequentially activated compartments (I = 0.6 mA, t = 5 min).

ACA-based electrochemical sensor development and characterization

The electrochemical sensors are fabricated on an ACA substrate, following a mediator-free enzymatic sensor development protocol. Our electrochemical sensing interface consists of an enzyme layer (glucose oxidase), a PPD layer, and a PtNP/Au layer (Fig. 3a). The PPD layer serves as a permselective membrane to reject interfering species in sweat matrix [21, 22], and the PtNP/Au layer facilitates the oxidation of the end-product (here, H_2O_2) generated from enzyme-catalyzed reaction. Similar sensor development protocols can be adopted to construct sensing interfaces targeting other biomarkers by incorporating suitable biorecognition and functional layers: for example, ACA-based lactate sensing interface can be created (Fig. S3) by utilizing lactate oxidase as a biorecognition layer, coupled with PVC as a functional layer (diffusion limiting).

The developed glucose sensors were first characterized, by capturing their amperometric responses (using a standard bench-top potentiostat) to a series of solutions with different glucose concentrations (spanning the typical glucose concentration range in sweat, 0-600 μM). As shown in Fig. 3b, the responses of the sensors to the glucose concentrations were highly linear (R^2 = 0.98).

The sensors' sensitivity and the limit of detection were 15.13 ± 0.8 μA/mM/cm^2 and 0.9 ± 0.05 μM, respectively. Furthermore, the amperometric sensor responses measured by the wireless FPCB were compared with those measured by the bench-top potentiostat. The results indicated that the corresponding FPCB and bench-top potentiostat readouts were closely matched (R^2 = 0.99, Fig. S4), thereby validating the FPCB's reliable signal acquisition, processing, and transmission capabilities.

To ensure reliable operation in complex biomatrices such as sweat, the selectivity performance of the glucose sensor was characterized by measuring its responses to a diverse panel of physiologically relevant interfering species, including electrolytes, electroactive species, drugs, sweat agonist, proteins, and other small molecules (listed in Fig. 3c). As shown in Fig. 3d, the response of the glucose sensor to the interfering species was negligible, while exhibiting step-wise current responses to glucose concentration increments.

To evaluate the sensors' preserved sensitivity for the duration of the envisioned on-body application (several hours), their amperometric responses were measured, in ambient conditions, every 2 hours. As illustrated in Fig. 3e, the sensors presented minimal sensitivity variations (Δ < 4.4 %) over the period of 10-hours.

Furthermore, the effect of mechanical deformation on the generated signal, along the sensor-circuit interconnection pathway (from the sensing interface to the FPCB contact pads), was characterized by recording the sensor-integrated FPCB's amperometric responses under different bending conditions (flat and α = 60°, R = 15 mm). As shown in Fig. S5, the induced bending had a negligible influence on the signal (< 5%). The constancy of the adhesion between the microfluidic sensor substrate (ACA) and the circuit board's contact pad was evaluated by

performing 180° peel adhesion test [23] as depicted in the inset of Fig. 3f, and was compared to the adhesion force between skin and the skin adhesive layer of the microfluidic module. As shown in Fig. 3f, the adhesion force between the skin and the skin adhesive layer was ~0.3 N/cm, meeting the skin adhesion limit (< 0.5 N/cm [24, 25]). The adhesion force between the microfluidic-sensing module's substrate and the circuit board metal contact pad was ~11.5 N/cm, indicating a relatively strong adhesion between the microfluidic and circuit modules (as compared to the adhesion force at the skin interface).

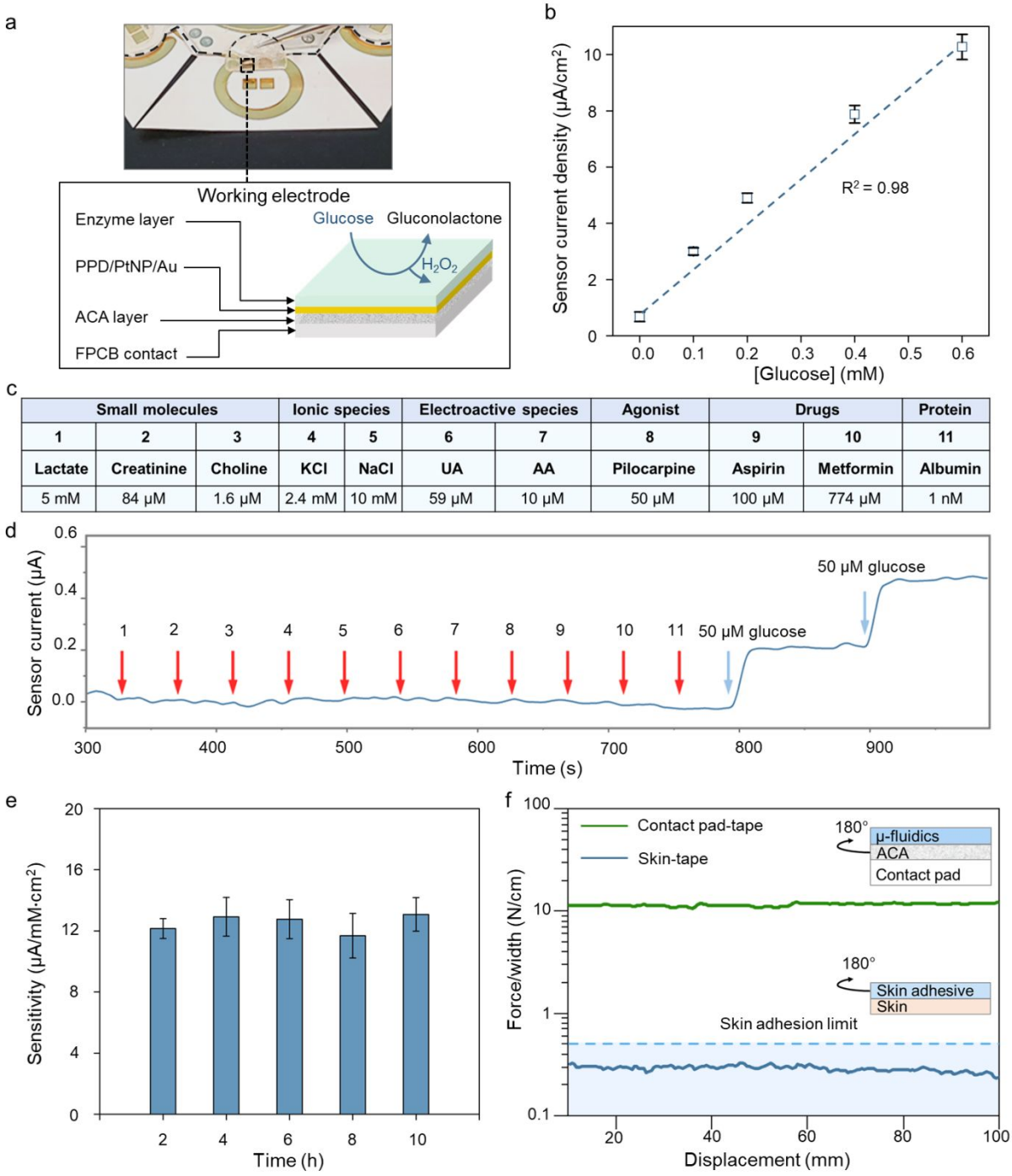

Small molecules			Ionic species		Electroactive species		Agonist	Drugs		Protein
1	2	3	4	5	6	7	8	9	10	11
Lactate	Creatinine	Choline	KCl	NaCl	UA	AA	Pilocarpine	Aspirin	Metformin	Albumin
5 mM	84 μM	1.6 μM	2.4 mM	10 mM	59 μM	10 μM	50 μM	100 μM	774 μM	1 nM

Figure 3. Characterization of the electrochemical sensing interface: a) Integration of the disposable microfluidic-sensing module onto the corresponding FPCB contact pad and illustration of the sensing layers/mechanism for the developed glucose sensor; b) The amperometric response of developed glucose sensors (n = 3 different sensors). Error bars indicate standard error (SE); c) Table of common interfering molecules in sweat used for the selectivity study; d) Selectivity study

for the glucose sensor by monitoring its response to the sequentially-introduced interferents and glucose. The arrows indicate the introduction time points for the corresponding interferents/glucose; e) The enzymatic sensors' preserved sensitivities over an 8-hour long storage at room temperature (SE, $n = 3$ different sensors); f) 180° peeling tests characterizing the adhesion force between the skin and tape, as well as PCB and tape. The inset demonstrates the setup of the 180° peeling test.

Integrated system for autonomous diurnal sweat sampling and analysis

The custom-developed wireless FPCB module integrates the required circuitries to implement system-level operations, including addressable and programmable iontophoretic-actuation and electrochemical sensor signal acquisition *via* six dedicated channels, as well as signal processing, and real-time biomarker data display (Fig. 4a, b). This FPCB can bilaterally communicate with a custom-developed smartphone application, *via* Bluetooth, to receive/transmit the command signals (to set the desired mode of operation for each of the compartments) and the biomarker data (Fig. S6). Upon processing the received command signals, the MCU automatically activates the iontophoretic circuitry and addresses the desired compartments (with the aid of multiplexers) to perform sweat stimulation at the intended time points (following the instructed iontophoresis settings). After the deactivation of the iontophoresis circuitry and following the MCU-generated instructions, the electrochemical sensing circuit continuously samples and processes the amperometric signal, thereby rendering biomarker data acquisition (Fig. S7, and supplementary methods).

The complete hybrid-flex system—consisting of the microfluidic-sensing and iontophoresis interfaces, integrated with the two-layered FPCB module—was deployed to acquire biomarker data at intermittent periods during the day and capture the biomarker's diurnal profile. Specifically, it was utilized to monitor the sweat glucose levels of a human subject over six

periods—before and after the consumption of three main meals during a day—where the sweat glucose readings during each period were captured by a designated compartment. Before and after each meal intake, sweat was iontophoretically stimulated for 5 minutes at 0.6 mA, and with the aid of the inbuilt pressure of the stimulated sweat glands, the harvested sweat sample was routed to and subsequently analyzed within the microfluidic sensing chamber of the same designated compartment (Fig. 4c). As shown in Fig. 4d, the changes in the baseline of the acquired diurnal sweat glucose profile reflected the elevation in glucose levels upon meal intake. This trend is aligned with previously reported observations, in which manual intervention was required to capture the glucose level for each time period [26].

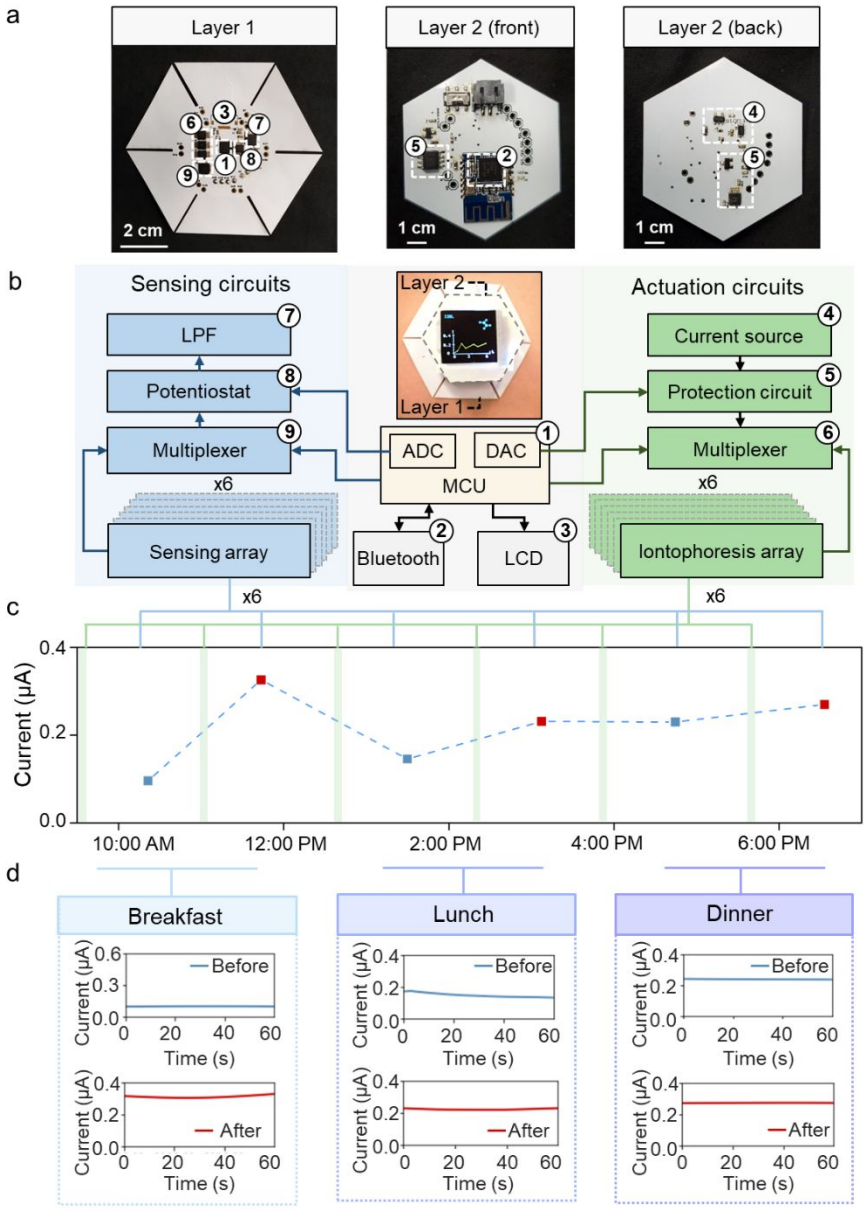

Figure 4. Integrated system for diurnal data acquisition: a) Optical images of the two-layered FPCB module. Layer 1 features the sensing circuitry (at the center) and iontophoretic electrode array (mechanically flexible flaps). Layer 2 features the iontophoretic circuitry and the data transmission/display interfaces; b) The system-level block diagram of the circuit operations; c) Diurnal sweat glucose profile (specifically, before and after main meal intakes, breakfast ~ 10:30 am, lunch ~ 2:00 pm, dinner ~ 5:30 pm), captured *via* on-body autonomous sweat sampling and analysis (by our system); d) Representative real-time amperometric recording of glucose sensors corresponding to the diurnal sweat glucose profile shown in Fig. 4c.

Conclusion

In conclusion, we devised a hybrid-flex multi-compartment autonomous wearable system, where each compartment can be activated, at desired time periods, to induce sweat—at programmable secretion rates—for *in-situ* biomarker analysis. To inform its clinical utility, we deployed this system in a human subject study aimed at tracking the diurnal sweat glucose profile, in which the results illustrated the elevation of sweat glucose upon the intake of each of the three main meals. The autonomous functionality and multi-compartment configuration of our solution eliminates the need for manual intervention for the device substitution (unlike the previously reported solutions requiring pristine microfluidic/sensor unit replacements to avoid sample/sensor contamination). Equivalently important, the demonstrated autonomous sweat acquisition and analysis capability can be exploited to adaptively sample contextual biomarker readings based on the user's need, behavior, and activity.

Furthermore, the generalizability of the introduced sensing system design and integration methodology allows for the integration of other electrochemical sensing interfaces to track the diurnal profiles of a wide panel of biomarkers. To this end, the previously reported wearable sensor development protocols can be leveraged, but may need to be optimized, to allow for sensor fabrication on an ACA substrate and vertical integration with our sensing system. Moreover, the mechanical flexibility of our device allows for its adherence to various body parts, enabling its use in clinical investigations aiming to study the correlation of sweat biomarker compositions secreted from different body sites. Additionally, the versatility of our system design allows for the incorporation of auxiliary sensing interfaces (*e.g.*, sweat pH, temperature), which could be helpful

in calibrating the sensor responses for more accurate biomarker level estimation and mitigating the confounding effects due to inter/intra-individual variations.

Toward translating this technology into personal health monitoring applications, large-scale and longitudinal studies are required to contextualize the diurnal sweat biomarkers' data in relation to the user's nutrition (composition, timing, and frequency of meal intakes), activities and other physiologically-relevant parameters. Augmenting data analytics techniques with the datasets harnessed by our scalable technology enables the establishment of clinical criteria to interpret sweat biomarkers' readings and provide actionable/personalized feedback to users. In this way, we can establish a non-invasive biomarker monitoring modality that can be scaled across the general population for personalized healthcare.

Author contributions

H.H., Y.Z., and S.E. conceived the idea and designed the experiments; H.H. led the experiments (with assistance from Y.Z., M.C.G., M.M., H.L., S.L., J.T., A.M.H., C.M., A.M.M., and S.E.); H.H., M.C.G., led the PCB design efforts; H.H., Y.Z., M.C.G., M.M., contributed analytic tools; H.H., Y.Z., M.C.G., M.M., H.L., S.L., J.T., A.M.H., C.M., A.M.M., and S.E. contributed to data analysis and interpretation; H.H., Y.Z., M.C.G., and S.E. drafted the manuscript and all the authors provided feedback. S.E. supervised the study.

Conflicts of interest

There are no conflicts to declare.

Acknowledgment

This work was supported by the National Science Foundation (Award No. 1722972), PATHS-UP's Faculty Innovation Seed Fund, PhRMA Foundation (Research Starter Grant in Translational Medicine and Therapeutics), Brain and Behavior Foundation (NARSAD Young Investigator Grant), H.H.'s Peter Staudhammer Northrop Grumman Fellowship, S.E.'s startup package (provided by the UCLA Henry Samueli School of Engineering and Applied Sciences), and the funding secured by the Preservation of the Force and Family Program at US Special Operations Command (executed as a sub-award issued to the University of California at Los Angeles by the Henry M. Jackson Foundation under a cooperative agreement with the Uniformed Services University). We extend gratitude to P. A. Deuster and Keiko Yabushita for providing feedback on the presented work and insightful discussions. We also thank Rona Jasmine Darabi

for her assistance with concept figure design. The authors appreciate the members of the UCLA Nanoelectronics Research Facility, Center for Minimally Invasive Therapeutics (C-MIT), and UCLA library for their help in device fabrication/characterization and instrumentation sharing.

References

1. A. Koh, D. Kang, Y. Xue, S. Lee, R. M. Pielak, J. Kim, T. Hwang, S. Min, A. Banks, P. Bastien, M. C. Manco, L. Wang, K. R. Ammann, K. I. Jang, P. Won, S. Han, R. Ghaffari, U. Paik, M. J. Slepian, G. Balooch, Y. Huang and J. A. Rogers, *Sci. Transl. Med.*, 2016, **8**, 366ra165.
2. W. Jia, A. J. Bandodkar, G. Valdés-Ramírez, J. R. Windmiller, Z. Yang, J. Ramírez, G. Chan and J. Wang, *Anal. Chem.*, 2013, **85**, 6553–6560.
3. W. Gao, S. Emaminejad, H. Y. Y. Nyein, S. Challa, K. Chen, A. Peck, H. M. Fahad, H. Ota, H. Shiraki, D. Kiriya, D. H. Lien, G. A. Brooks, R. W. Davis and A. Javey, *Nature*, 2016, **529**, 509–514.
4. H. Lee, C. Song, Y. S. Hong, M. S. Kim, H. R. Cho, T. Kang, K. Shin, S. H. Choi, T. Hyeon and D. H. Kim, *Sci. Adv.*, 2017, **3**, e1601314.
5. S. Emaminejad, W. Gao, E. Wu, Z. A. Davies, H. Y. Y. Nyein, S. Challa, S. P. Ryan, H. M. Fahad, K. Chen, Z. Shahpar, S. Talebi, C. Milla, A. Javey and R. W. Davis, *Proc. Natl. Acad. Sci. U. S. A.*, 2017, **114**, 4625–4630.
6. W. Gao, H. Y. Y. Nyein, Z. Shahpar, H. M. Fahad, K. Chen, S. Emaminejad, Y. Gao, L. C. Tai, H. Ota, E. Wu, J. Bullock, Y. Zeng, D. H. Lien and A. Javey, *ACS Sensors*, 2016, **1**, 866–874.
7. B. Schazmann, D. Morris, C. Slater, S. Beirne, C. Fay, R. Reuveny, N. Moyna and D. Diamond, *Anal. Methods*, 2010, **2**, 342–348.
8. J. Kim, I. Jeerapan, S. Imani, T. N. Cho, A. Bandodkar, S. Cinti, P. P. Mercier and J. Wang, *ACS Sensors*, 2016, **1**, 1011–1019.
9. A. J. Bandodkar, D. Molinnus, O. Mirza, T. Guinovart, J. R. Windmiller, G. Valdés-Ramírez, F. J. Andrade, M. J. Schöning and J. Wang, *Biosens. Bioelectron.*, 2014, **54**, 603–609.
10. A. J. Bandodkar, V. W. S. Hung, W. Jia, G. Valdés-Ramírez, J. R. Windmiller, A. G. Martinez, J. Ramírez, G. Chan, K. Kerman and J. Wang, *Analyst*, 2013, **138**, 123–128.

11. W. Gao, H. Y. Y. Nyein, Z. Shahpar, H. M. Fahad, K. Chen, S. Emaminejad, Y. Gao, L. C. Tai, H. Ota, E. Wu, J. Bullock, Y. Zeng, D. H. Lien and A. Javey, *ACS Sensors*, 2016, **1**, 866–874.

12. W. Gao, H. Y. Y. Nyein, Z. Shahpar, H. M. Fahad, K. Chen, S. Emaminejad, Y. Gao, L. C. Tai, H. Ota, E. Wu, J. Bullock, Y. Zeng, D. H. Lien and A. Javey, *ACS Sensors*, 2016, **1**, 866–874.

13. *MACRODUCT SWEAT COLLECTION SYSTEM instruction/service manual Model 3700 SYS*, 2004.

14. D. M. Sletten, K. Kimpinski, S. D. Weigand and P. A. Low, *Auton. Neurosci. Basic Clin.*, 2009, **150**, 127–130.

15. C. Boehler, T. Stieglitz and M. Asplund, *Biomaterials*, 2015, **67**, 346–353.

16. X. Cheng, B. Wang, Y. Zhao, H. Hojaiji, S. Lin, R. Shih, H. Lin, S. Tamayosa, B. Ham, P. Stout, K. Salahi, Z. Wang, C. Zhao, J. Tan and S. Emaminejad, *Adv. Funct. Mater.*, 2020, **30**, 1908507.

17. R. M. Fish and L. A. Geddes, *Eplasty*, 2009, **9**.

18. Clinical and Laboratory Standards Institute, *CLSI*, 2009, **29**, C34-A3.

19. H. Lin, J. Tan, J. Zhu, S. Lin, Y. Zhao, W. Yu, H. Hojaiji, B. Wang, S. Yang, X. Cheng, Z. Wang, E. Tang, C. Yeung and S. Emaminejad, *Nat. Commun*., 2020, 11, 4405.

20. J. Tan, H. Lin, S. Lin, W. Yu, J. Zhu, Y. Zhao, X. Cheng, S. Yang, E. Tang and S. Emaminejad, *J. Microelectromechanical Syst*., 2020, 1–3.

21. B. Wang, B. Koo, L. W. Huang and H. G. Monbouquette, *Analyst*, 2018, **143**, 5008–5013.

22. X. Wen, B. Wang, S. Huang, T. “Leo” Liu, M. S. Lee, P. S. Chung, Y. T. Chow, I. W. Huang, H. G. Monbouquette, N. T. Maidment and P. Y. Chiou, *Biosens. Bioelectron.*, 2019, **131**, 37–45.

23. Y. Zhao, B. Wang, H. Hojaiji, Z. Wang, S. Lin, C. Yeung, H. Lin, P. Nguyen, K. Chiu, K. Salahi, X. Cheng, J. Tan, B. A. Cerrillos and S. Emaminejad, *Sci. Adv.*, 2020, **6**, eaaz0007.

24. J. Kim, Y. Hwang, S. Jeong, S. Y. Lee, Y. Choi and S. Jung, *J. Mater. Chem. C*, 2018, **6**, 2210–2215.

25. L. Liu, K. Kuffel, D. K. Scott, G. Constantinescu, H. J. Chung and J. Rieger, *Biomed. Phys. Eng. Express*, DOI:10.1088/2057-1976/aa91fb.

26. H. Lee, T. K. Choi, Y. B. Lee, H. R. Cho, R. Ghaffari, L. Wang, H. J. Choi, T. D. Chung, N. Lu, T. Hyeon, S. H. Choi and D. H. Kim, *Nat. Nanotechnol.*, 2016, **11**, 566–572.

We present a hybrid-flex wearable system to autonomously analyze sweat—induced at programmable secretion rates—for diurnal biomarker data acquisition.